pH-regulated Antimony Oxychloride Nanoparticle Formation on Titanium Oxide Nanostructures: A Photocatalytically Active Heterojunction

Balázs Buchholcz,[1] Henrik Haspel,[1] Tamás Boldizsár,[1] Ákos Kukovecz[1,2] and Zoltán Kónya[1,3*]

[1]Department of Applied and Environmental Chemistry, University of Szeged, H-6720 Szeged, Rerrich Béla tér 1, Hungary;
[2]MTA-SZTE "Lendület" Porous Nanocomposites Research Group, H-6720 Szeged, Rerrich Béla tér 1, Hungary;
[3]MTA-SZTE Reaction Kinetics and Surface Chemistry Research Group, H-6720 Szeged, Rerrich Béla tér 1, Hungary;
*****Corresponding author: konya@chem.u-szeged.hu; Tel.: +36-62-544-620

Supplementary Data

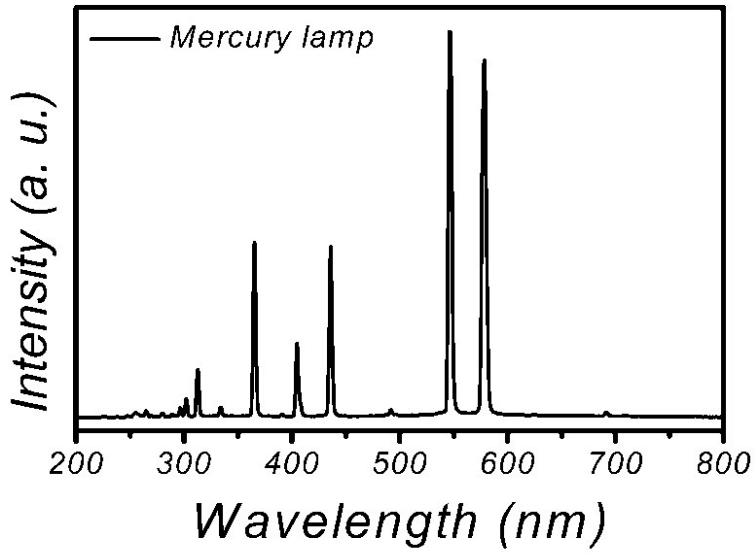

Fig. S1. UV-VIS spectrum of the mercury vapor light source used in the photocatalytic dye decomposition test reactions.

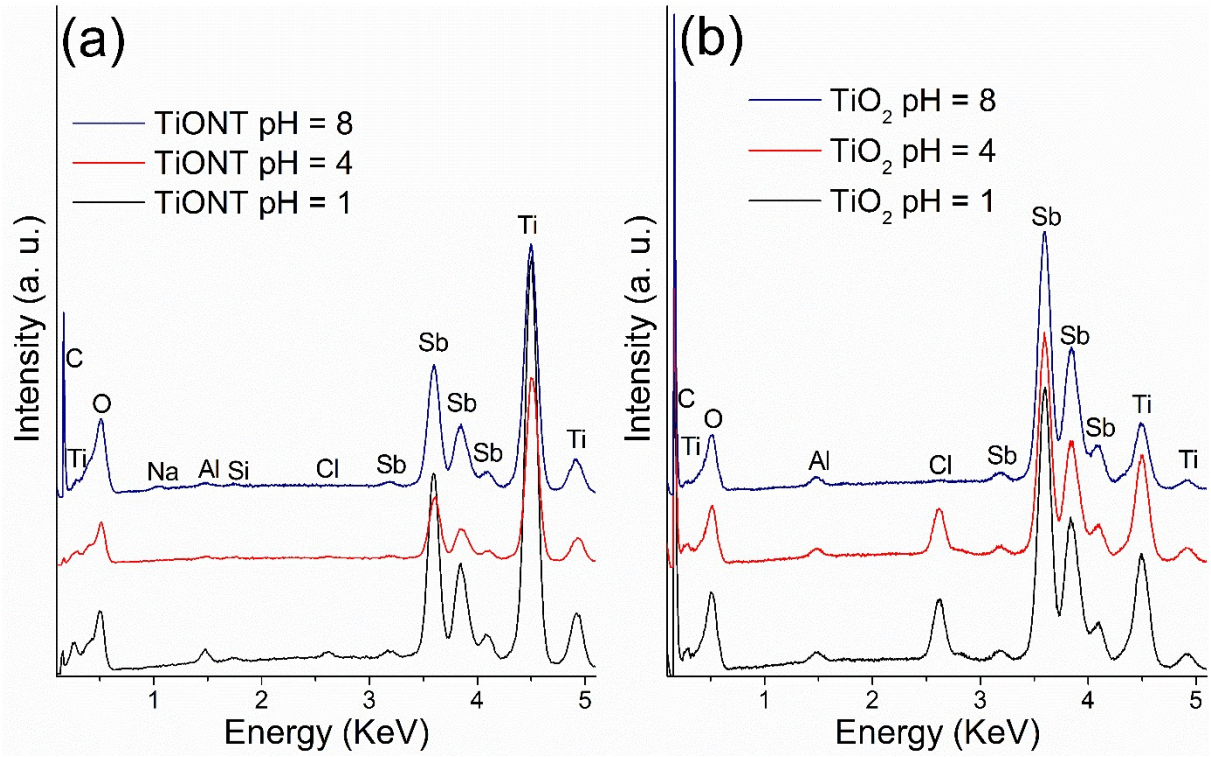

Fig. S2. EDS spectra of the $Sb_xO_yCl_z$ decorated TiONT composites. The presence of antimony is clearly seen in all spectra.

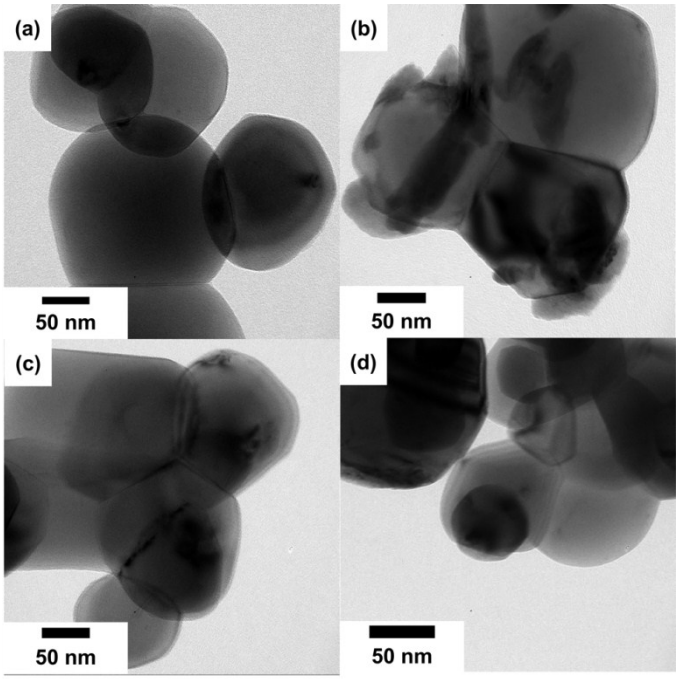

Fig. S3. TEM images of the pristine anatase TiO_2 nanoparticles (a), and nanoparticles decorated with $Sb_xO_yCl_z$ synthesized at pH = 1 (b), 4 (c), and 8 (d). The corresponding particle size distributions cannot be determined from TEM images.

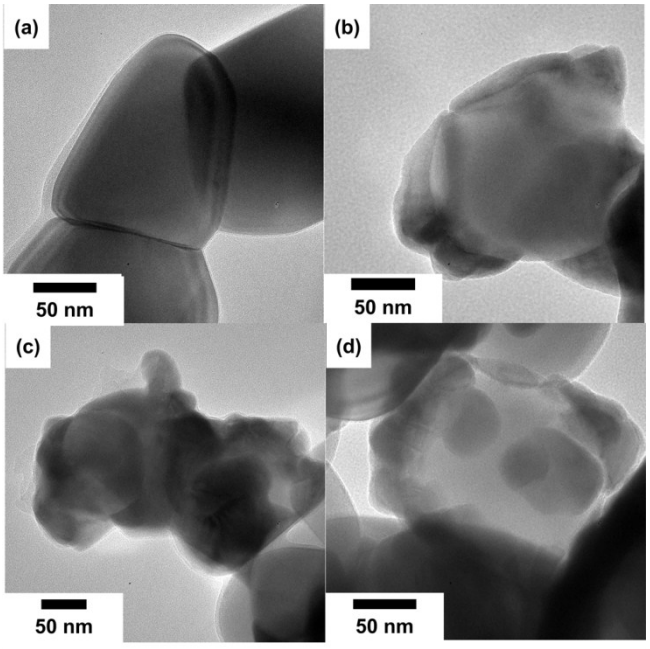

Fig. S4. TEM images of the pristine anatase TiO_2 nanoparticles (a), and nanoparticles decorated with $Sb_xO_yCl_z$ synthesized at pH = 1 (b), 4 (c), and pH 8 (d) after heat treatment at 400 °C in air atmosphere for 1 hour. The corresponding particle size distributions cannot be determined from TEM images.

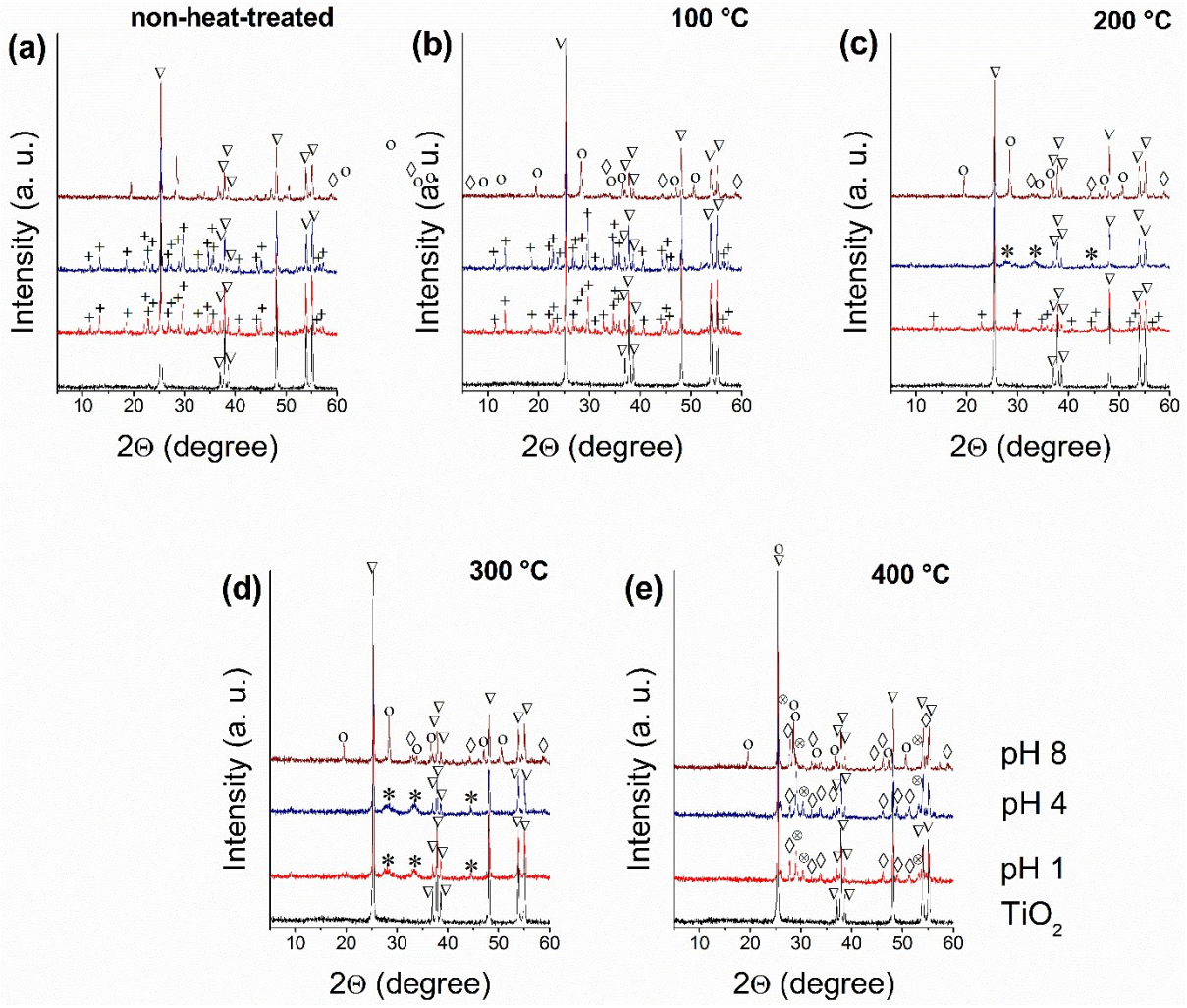

Fig. S5. XRD patterns of the as-prepared (a) and the heat treated TiO_2 samples calcined at 373 K (b), 473 K (c), 573 K (d), and 673 K (e). Anatase phase is marked by "∇". The symbol "+" belongs to $Sb_8O_{11}Cl_2(H_2O)_6$, "*" to $Sb_8O_{11}Cl_2$, "o" to valentinite Sb_2O_3, ◊ to senarmontite Sb_2O_3, and ⊗ to the cervantite Sb_2O_4.

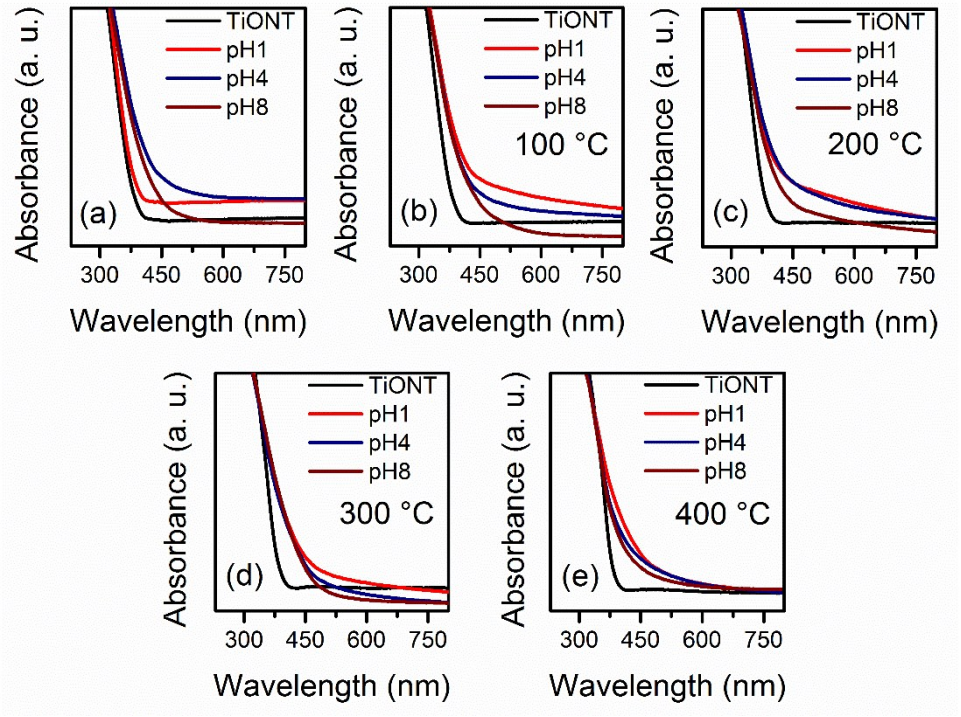

Fig. S6. Diffuse reflectance UV-VIS spectra of the $Sb_xO_yCl_z$/TiONT composites before heat treatment (a), after calcination at 100 (b), 200 (c), 300 (d), and 400 °C (e) in air for 1 hour.

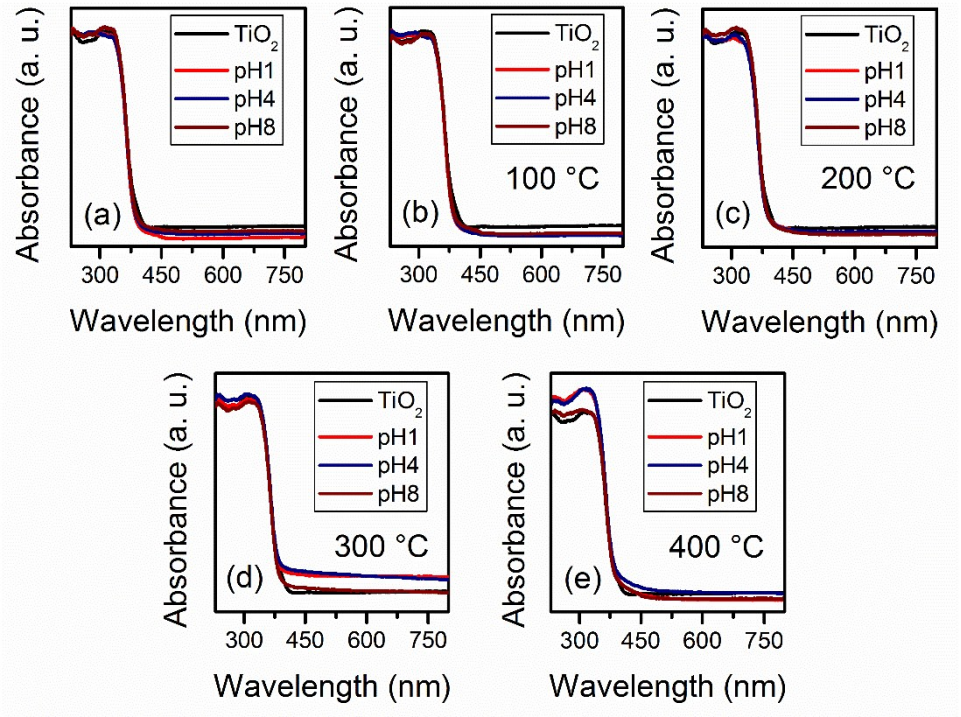

Fig. S7. Diffuse reflectance UV-VIS spectra of the $Sb_xO_yCl_z/TiO_2$ composites before heat treatment (a), after calcination at 100 (b), 200 (c), 300 (d), and 400 °C (e) in air for 1 hour.

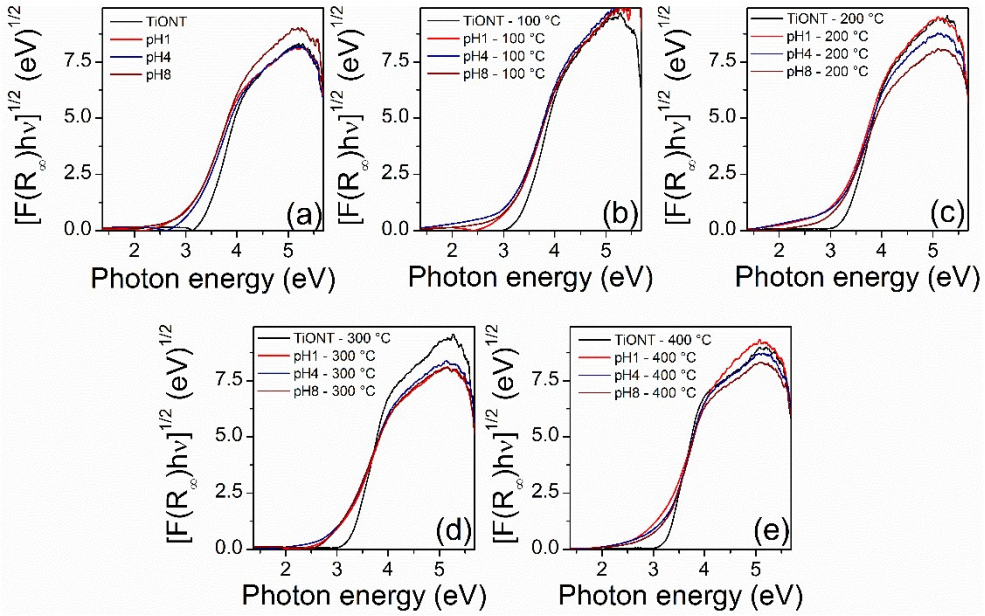

Fig. S8. Diffuse reflectance UV-VIS spectra in the Kubleka-Munk formalism of the $Sb_xO_yCl_z$/TiONT composites before heat treatment (a), after calcination at 100 (b), 200 (c), 300 (d), and 400 °C (e) in air for 1 hour.

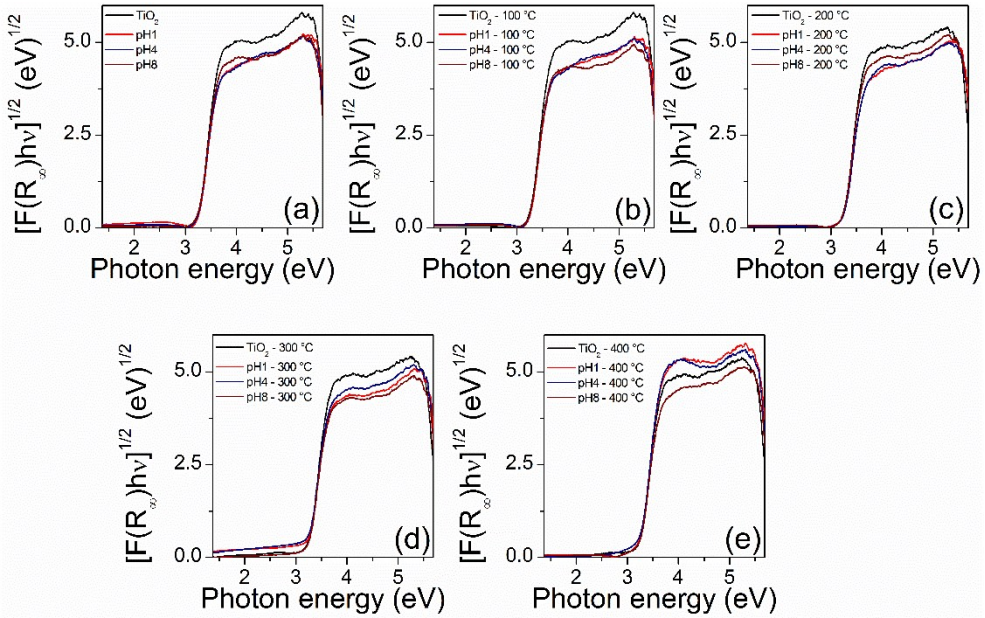

Fig. S9. Diffuse reflectance UV-VIS spectra in the Kubleka-Munk formalism of the $Sb_xO_yCl_z/TiO_2$ composites before heat treatment (a), after calcination at 100 (b), 200 (c), 300 (d), and 400 °C (e) in air for 1 hour.

Table S1

Optical band gap energies of the $Sb_xO_yCl_z$/TiONT composites before and after calcination.

	Band gap energy (eV)				
Samples	TiONT	pH1	pH4	pH8	Average
No calcination	3.36	3.04	3.08	3.04	3.05 ± 0.02
100 °C	3.37	3.12	3.04	3.12	3.09 ± 0.05
200 °C	3.28	3.10	3.10	3.11	3.10 ± 0.01
300 °C	3.28	3.02	3.00	2.98	3.00 ± 0.02
400 °C	3.25	3.13	3.20	3.18	3.17 ± 0.04

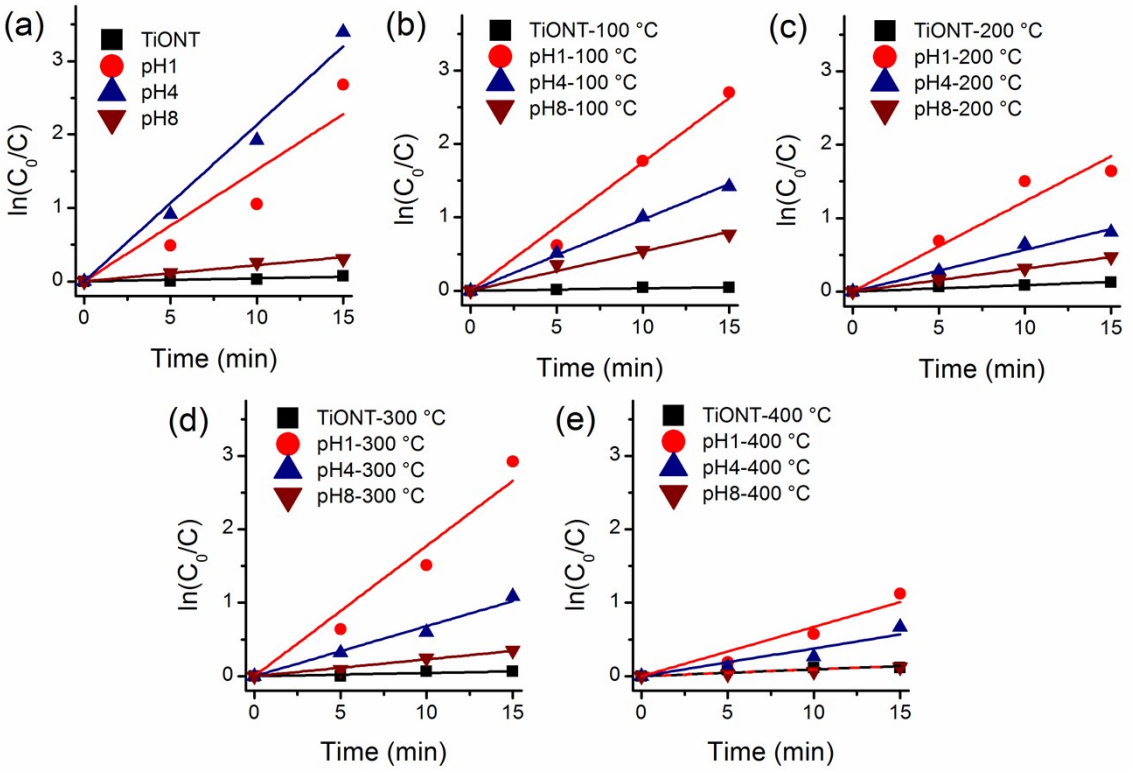

Fig. S10. Photocatalytic dye decomposition curves of methyl orange (MO) under UV-VIS irradiation using $Sb_xO_yCl_z$/TiONT composites. As-prepared composites (a), composites heat treated at 100 (b), 200 (c), 300 (d), and 400 °C (e) in air for 1 hour.

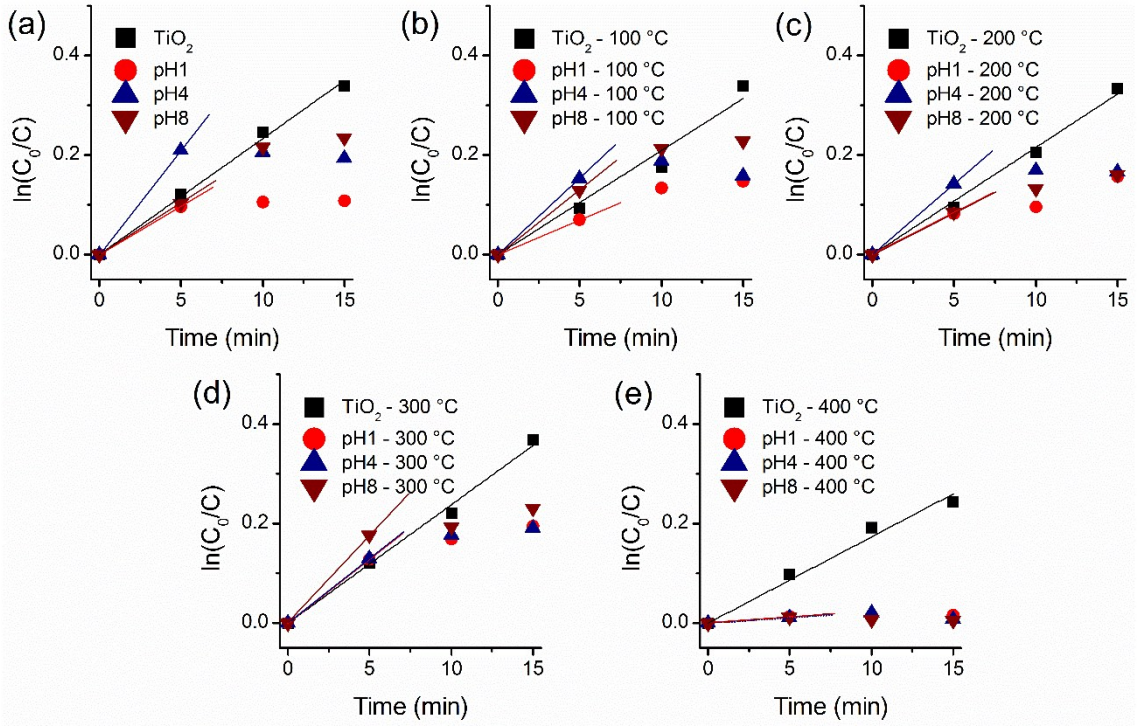

Fig. S11. Photocatalytic dye decomposition curves of methyl orange (MO) under UV-VIS irradiation using $Sb_xO_yCl_z/TiO_2$ composites.

Table S2
First-order apparent rate constants of the MO decolorization reaction in the $Sb_xO_yCl_z$/TiONT composites.

	Apparent rate constant (x10^{-3} min^{-1})			
Samples	TiONT	pH1	pH4	pH8
No calcination	4.09	151.75	213.21	22.02
100 °C	3.26	174.94	96.90	53.51
200 °C	8.83	123.03	56.93	31.37
300 °C	4.37	177.49	68.17	22.96
400 °C	9.25	67.21	40.59	7.37

Table S3
First-order apparent rate constants of the MO decolorization reaction in the $Sb_xO_yCl_z/TiO_2$ composites.

	Apparent rate constant (x10^{-3} min^{-1})			
Samples	TiO_2	pH1	pH4	pH8
No calcination	27.30	13.00	21.10	17.70
100 °C	24.89	15.10	18.30	17.70
200 °C	25.51	14.50	18.00	11.90
300 °C	27.79	19.00	19.00	18.00
400 °C	21.31	1.00	2.90	0.30

Table S4
Photocatalytic properties of various photocatalysts in methyl orange decolorization experiments.

Photocatalyst	Photocatalytic activity	Reference photocatalyst and its activity	Enhancement factor	Ref.
$Sb_2S_3/Sb_4O_5Cl_2$	83% (VIS) in 1h	$Sb_4O_5Cl_2$: 1%	83	[1]
$Sb_2S_3/g\text{-}C_3N_4$	70% (NIR) in 2h	Sb_2S_3: 36%	1.9	[2]
	58% (UV) in 1h	Sb_2S_3: 17%	3.4	
	82% (VIS) in 1h	Sb_2S_3: 20%	4.1	
$gCN\text{-}Sb_2S_3/Sb_4O_5Cl_2$	95% (VIS) in 1h	$g\text{-}C_3N_4$: 6%	15.8	[3]
BiOCl (001)	99% (UV) in 45 min	no catalyst (UV): 13%	7.6	[4]
	5% (VIS) in 3h		1.7	
BiOCl (010)	59% (UV) in 45 min	no catalyst (VIS): 3%	4.5	
	33% (VIS) in 3h		11	
BiOCl	100% (VIS) in 10 min	no catalyst: 1%	100	[5]
$Bi_7F_{11}O_5/BiOCl$	80% (UV) in 30 min	BiOCl: 39%	2.1	[6]
BIOI	82% (VIS) in 2h	-	-	[7]
$g\text{-}C_3N_4/BiOI$	92% (VIS) in 2h	-	-	
$BiOI/TiO_2$	92% (VIS) in 3h	TiO_2: 4%	23	[8]

The method for determining band edge values was described earlier by X. Xiao et al. (X. Xiao, S. Tu, M. Lu, H. Zhong, C. Zheng, X. Zuo and J. Nan, Appl. Catal., B, 2016, **198**, 124–132.). Briefly, the flat band potential of the pH1 sample was determined by electrochemical impedance spectroscopy (EIS) in 0.5 M Na_2SO_4 solution in a three-electrode configuration using an ACM Instruments Gill AC electrochemical workstation. Pt foil as the counter electrode and Ag/AgCl (3M KCl) reference electrode were used for the measurements. All potentials in the study refer to the normal hydrogen electrode (NHE) potential. The working electrode were prepared by drop-casting on a glassy carbon electrode (3 mm in diameter) surface. The impedance was measured at a constant frequency varying the applied potential. The capacitance of the space charge layer can be determined by equation (1) where Z_{im} is the imaginary part of measured Z^* impedance, i is imaginary unit, and f is the ac-voltage frequency:

$$C_{sc} = \frac{-i}{2\pi f Z_{im}} \quad (1)$$

For the determination of the flat band potential, C^{-1} from Eq. 1 was depicted against the

applied potential, and the linear range of the dataset were fitted. Fig. S12. shows the resulted Mott-Schottky plot.

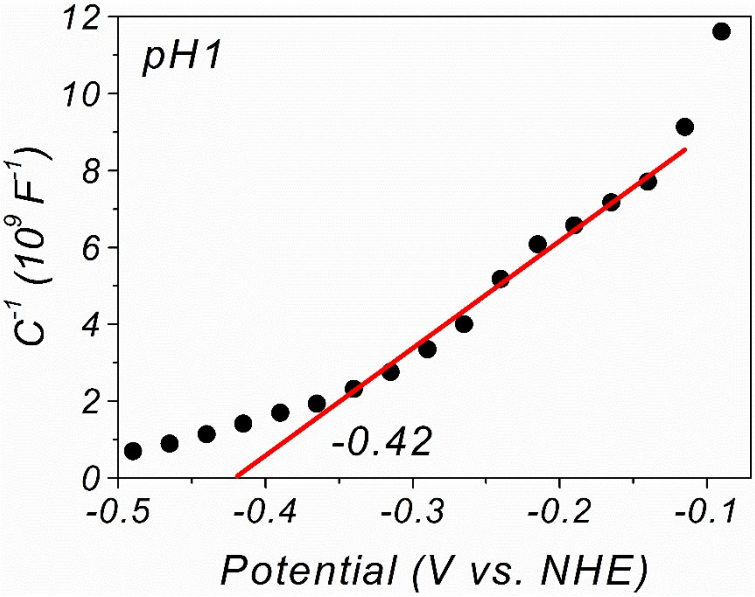

Fig. S12. Mott-Schottky plot of the $Sb_xO_yCl_z$/TiONT composite prepared at pH = 1, measured at 500 Hz frequency in 0.5 M Na_2SO_4 aqueous solution.

The intercept with the x axis gives the position of the conduction band of $Sb_4O_5Cl_2$ under flat band condition. Since the conduction band position and the band gap energy (from UV-Vis spectroscopy) is known, the position of the valence band can be calculated from the following equation:

$$E_{\text{Conduction Band}} - E_{\text{Band Gap}} = E_{\text{Valence Band}} \quad (2)$$

Band diagrams are based by on review of Bai et al.:
S. Bai, J. Jiang, Q. Zhang and Y. Xiong, *Chem. Soc. Rev.*, 2015, **44**, 2893-2939

References

[1] Q. Jiang, X. Yuan, H. Wang, X. Chen, S. Gu, Y. Liu, Z. Wu, G. Zeng, A facile hydrothermal method to synthesize Sb_2S_3/$Sb_4O_5Cl_2$ composites with three-dimensional spherical structures, RSC Adv. 5 (2015) 53019-53024.

[2] H. Wang, X. Yuan, H. Wang, X. Chen, Z. Wu, L. Jiang, W. Xiong, G. Zeng, Facile synthesis of Sb_2S_3/ultrathin g-C_3N_4sheets heterostructures embedded with g-C_3N_4 quantum

dots with enhanced NIR-light photocatalytic performance, App. Catal. B 193 (2016) 36-46.

[3] Y. Liu, X. Yuan, H. Wang, X. Chen, S. Gu, Q. Jiang, Z. Wu, L. Jiang, Y. Wu, G. Zeng, Novel visible light-induced g-C_3N_4-Sb_2S_3/$Sb_4O_5Cl_2$ composite photocatalysts for efficient degradation of methyl orange, Catal. Comm. 70 (2015) 17-20.

[4] J. Jiang, K. Zhao, X. Xiao, L. Zhang, Synthesis and Facet-Dependent Photoreactivity of BiOCl Single-Crystalline Nanosheets, J. Am. Chem. Soc. 134 (2012) 4473-4476.

[5] K. Zhang, C. Liu, F. Huang, C. Zheng, W. Wang, Study of the electronic structure and photocatalytic activity of the BiOCl photocatalyst, App. Catal. B 68 (2006) 125-129.

[6] Y. Kan, Y. Yang, F. Teng, L. Yang, J. Xu, Y. Teng, Synthesis of $Bi_7F_{11}O_5$/BiOCl nanosheets by a simple post-synthesis method and the improved charge separation by the heterojunction, Catal. Comm. 87 (2016) 10-13.

[7] J. Di, J. Xi, S. Yin, H. Xu, L. Xu, Y. Xu, M. He, H. Li Preparation of sphere-like g-C_3N_4/BiOI photocatalysts via a reactable ionic liquid for visible-light-driven photocatalytic degradation of pollutants J. Mater. Chem. A 2 (2014) 5340-5351.

[8] K. Wang, C. Shao, X. Li, F. Miao, N. Lu, Y. Liu, Heterojunctions of p-BiOI Nanosheets/n-TiO_2 Nanofibers: Preparation and Enhanced Visible-Light Photocatalytic Activity, Materials 9 (2016) 90.